IOP Publishing Journal of Physics: Condensed Matter

J. Phys.: Condens. Matter **19** (2007) 255210 (14pp) doi:10.1088/0953-8984/19/25/255210

Bipolaron formation in 1D–3D quantum dots: a lattice quantum Monte Carlo approach

M Hohenadler[1] **and H Fehske**[2]

[1] Theory of Condensed Matter, Cavendish Laboratory, Cambridge, UK
[2] Institute for Physics, Ernst-Moritz-Arndt University Greifswald, Germany

E-mail: mh507@cam.ac.uk

Received 15 September 2006, in final form 21 November 2006
Published 30 May 2007
Online at stacks.iop.org/JPhysCM/19/255210

Abstract

Polaron and bipolaron formation in the Holstein–Hubbard model with harmonic confinement potential, relevant to quantum dot structures, is investigated in one to three dimensions by means of unbiased quantum Monte Carlo simulations. The discrete nature of the lattice and quantum phonon effects are fully taken into account. The dependence on phonon frequency, Coulomb repulsion, confinement strength (dot size) and electron–phonon interaction strength is studied over a wide range of parameter values. Confinement is found to reduce the size of (bi-)polarons at a given coupling strength, to reduce the critical coupling for small-(bi-)polaron formation, to increase the polaron binding energy, and to be more important in lower dimensions. The present method also permits one to consider models with dispersive phonons, anharmonic confinement, or long-range interactions.

1. Introduction

Continuous advances in fabrication methods in semiconductor physics over recent decades have enabled researchers to create nanoscale systems in which carrier motion is confined along one or more spatial dimensions. Among these structures are quantum dots [1, 2], corresponding to quasi-zero-dimensional systems with some atom-like properties [3], which are of substantial technical interest due to their potential use as lasers [4], in quantum computing [5], as storage devices [6], or as single-photon sources [7, 8]. Improvements in experimental techniques now also permit studies of the properties of individual dots rather than ensembles [9], as well as of molecular quantum dots [10].

Apart from strong correlations between electrons, the interaction of charge carriers with the lattice degrees of freedom is of great relevance, especially concerning its role in dephasing and relaxation processes [11–13] as well as transport [14]. Evidence for the existence of polarons (carriers bound to a self-induced lattice distortion) has been given [15], and non-trivial multi-phonon effects and polaron formation have been proposed to explain the lack of experimental

evidence for the phonon bottleneck in quantum dots [11, 16]. Formation of bipolarons (bound electron pairs sharing a phonon cloud) has been proposed as an explanation for pair tunnelling from GaAs quantum dots [17]. Besides, (small) bipolaron states significantly influence the transport through single molecules [18, 19].

The problem of polaron formation in a quantum dot has received a lot of attention in the past (see [20–24] and references therein). From this work, the general conclusion is that confinement enhances the tendency of an electron to undergo a crossover to a (small) polaron so that heavy polaronic quasiparticles may be realized experimentally even in the weak or intermediate electron–phonon coupling regime. Less work has been devoted to understand bipolaron formation in quantum dots [17, 23–26], with contradictory results on the effect of confinement [23, 26].

All existing work is based on the continuum Fröhlich model [27], employing mainly variational approaches of different reliability—the above-mentioned conflicting results seem to originate from the inadequacy of some of the approaches used. However, from a theoretical point of view, the most interesting case is that in which the extension of the lattice displacement attached to the charge carriers is comparable to the confinement length. The Holstein molecular-crystal model was originally developed [28] to answer the question as to whether a local lattice instability occurs upon increasing the electron–phonon coupling. This problem cannot be addressed in the framework of continuum models, since the local lattice dynamics on the scale of the unit cell has to be taken into account [29].

The need for lattice models also stems from the fact that it is nowadays possible to fabricate self-assembled quantum dots with lateral dimensions of less than 4 nm [9], which contain only a small number of unit cells in each direction. Obviously, in such systems, the discrete nature of the lattice will play an important role, motivating us to revisit the problem of (bi-)polaron formation.

The Holstein–Hubbard model considered here is not completely realistic, as it only includes local electron–phonon and electron–electron interactions as well as a coupling to dispersionless optical phonons. However, we are interested in fundamental effects arising from the combination of electron–phonon interaction and confinement in discrete systems. Besides, many aspects of quantum dots may be understood using effective models [1].

From numerous studies of Holstein models with one (two) electrons on a discrete lattice [30, 31], it is well known that the nonlinear process of (bi-)polaron formation represents a complex many-body problem that may not be satisfactorily described by means of variational or perturbative approaches. The necessity for a universal all-coupling approach to describe intermediate-coupling materials such as CdTe was pointed out long ago [21], motivating the application of unbiased numerical methods.

In this work, we extend the world-line quantum Monte Carlo (QMC) method of [32–35] to include a harmonic confining potential. The method yields practically exact and unbiased results in any dimension, in principle with no restrictions of system size or parameters. As a consequence, we will be able to study (bi-)polaron formation over the whole range from weak to strong confinement. The method is capable of treating systems with long-range interactions or dispersive phonons, which opens up interesting perspectives for future work. An important finding as compared to previous work (including [36]) concerns the problem of very long autocorrelations times in certain parameter regimes. Finally, in contrast to earlier Green function QMC calculations for a continuum model [17], the present approach does not rely on a trial wavefunction.

The paper is organized as follows. In section 2, we present the model and briefly discuss the underlying approximations. The QMC method is described in sections 3, and 4 contains a discussion of our results. We end with a summary and an outlook for future work in section 5.

2. Model

We consider a Holstein–Hubbard model, supplemented by a harmonic confining potential. Using dimensionless phonon variables, the Hamiltonian reads

$$H = \underbrace{-t \sum_{\langle i,j\rangle\sigma} c^{\dagger}_{i\sigma} c_{j\sigma}}_{H_{\rm kin}} + \underbrace{U \sum_i \hat{n}_{i\uparrow}\hat{n}_{i\downarrow}}_{H_{\rm ee}} + \underbrace{K \sum_i |\boldsymbol{r}_i|^2 \hat{n}_i}_{H_{\rm con}} + \underbrace{\frac{\omega_0}{2} \sum_i \left(\hat{p}_i^2 + \hat{x}_i^2\right)}_{H_{\rm ph}=H^p_{\rm ph}+H^x_{\rm ph}} \underbrace{- \alpha \sum_i \hat{x}_i \hat{n}_i}_{H_{\rm ep}} . \quad (1)$$

Here $c^{\dagger}_{i\sigma}$ creates an electron of spin σ on lattice site i, and $H_{\rm kin}$ describes the hopping of electrons between nearest-neighbouring lattice sites $\langle i, j\rangle$ with hopping integral t. The second term, $H_{\rm ee}$, accounts for on-site Coulomb repulsion between electrons, where $\hat{n}_{i\sigma} = c^{\dagger}_{i\sigma} c_{i\sigma}$. The harmonic confinement potential, its strength being measured by K, is given by $H_{\rm con}$, $\boldsymbol{r}_i$ denotes the position vector of an electron at site i, and $\hat{n}_i = \sum_\sigma \hat{n}_{i\sigma}$. $H_{\rm ph}$ constitutes the kinetic $H^p_{\rm ph}$ and potential energy $H^x_{\rm ph}$ energy of the lattice degrees of freedom, corresponding to independent harmonic oscillators with energy ω_0. Finally, $H_{\rm ep}$ mediates the coupling between the local electron occupation $\hat{n}_i$ and the lattice distortion $\hat{x}_i$ with coupling strength α. We use units such that $\hbar = k_{\rm B} = e = 1$, consider D-dimensional hypercubic lattices of linear size N and volume $N^{\rm D}$, and assume periodic boundary conditions in real space.

In terms of the coupling parameter α, the atomic-limit ($t = 0$) polaron binding energy $E_{\rm P}$ is given by $E_{\rm P} = \alpha^2/(2\omega_0)$. We define the usual dimensionless coupling constant $\lambda = 2E_{\rm P}/W$, with the free bandwidth $W = 4tD$. Furthermore, we introduce the adiabaticity ratio $\gamma = \omega_0/t$, which permits us to distinguish between the adiabatic ($\gamma < 1$) and the non-adiabatic ($\gamma > 1$) regimes.

This paper is exclusively concerned with the cases of either one electron, or two electrons of opposite spin forming a spin singlet. Obviously, for $N_{\rm e} = 1$, $H_{\rm ee} = 0$ and spin indices may be dropped. In experiments, the maximum number of electrons in a quantum dot is strongly influenced by the dot size (set here by K), so that the low-density regime considered here may be relevant in particular for small dots, which are of interest due to their potential use as quantum bits [6]. One- and two-electron states also play an important role in molecular transistors, corresponding (in the simplest case) to a quantum dot with a single electronic level coupled to a vibrational mode [18, 19].

As we are interested in fundamental effects due to confinement, the Holstein–Hubbard-type model seems a good starting point, especially as a lot of knowledge is available for $K = 0$ [35, 37–40]. Although quantitative results for realistic quantum dot systems are beyond the scope of this work, let us briefly discuss the simplifications inherent to the Hamiltonian (1).

Using a one-band model we ignore the existence of a band gap in semiconducting host materials. Hence, our considerations are restricted to one or two carriers in the same (either conduction or valence) band. A symmetric, parabolic confining potential—which can be realized experimentally [1]—is assumed for simplicity, although more general situations may be studied.

We restrict ourselves to a simple effective electron–phonon coupling to a dispersionless (optical) phonon branch. For such local phonon modes, and in the absence of sharp interfaces, the bulk-phonon approximation is expected to be a good starting point. The coupling to optical phonons has been shown to dominate bipolaron formation [17].

The Hamiltonian (1) only contains on-site interactions, which are not completely justified in the case of semiconducting materials. Long-range interactions will be the subject of future investigations.

3. Method

The QMC method used here is a straightforward extension of [32, 33, 35]. The appealing features of this approach are the analytical integration over the phonon degrees of freedom—enabling us to study the adiabatic regime—and the fact that the numerical effort is essentially independent of system size. Besides, the formalism treats the cases of one and two electrons on the same footing, and is general enough so as to permit future studies of models with, for example, dispersive phonons or long-range interactions.

3.1. Partition function

The derivation of the relevant fermionic contribution Z^{f} (the bosonic part can be calculated exactly) to the partition function $Z = \mathrm{Tr}\,\mathrm{e}^{-\beta H}$ is almost identical to [33, 35]. Dividing the imaginary-time axis $[0, \beta]$ ($\beta = (k_{\mathrm{B}}T)^{-1}$ is the inverse temperature) into intervals of length $\Delta\tau = \beta/L \ll 1$, we may write

$$Z_L \approx \mathrm{Tr}[\mathrm{e}^{-\Delta\tau(H_{\mathrm{kin}}+H_{\mathrm{con}})}\mathrm{e}^{-\Delta\tau(H^x_{\mathrm{ph}}+H_{\mathrm{ep}})}\mathrm{e}^{-\Delta\tau H^p_{\mathrm{ph}}}]^L. \tag{2}$$

The result for the partition function reads [33]

$$Z^{\mathrm{f}}_L = \sum_{\{\boldsymbol{r}^{(\xi)}_\tau\}} w^{\mathrm{f}}(\{\boldsymbol{r}^{(\xi)}_\tau\}), \tag{3}$$

with the fermionic weight

$$w^{\mathrm{f}}(\{\boldsymbol{r}^{(\xi)}_\tau\}) = \exp\left\{\sum_{\tau,\tau'=1}^{L} F(\tau-\tau')\sum_{\xi,\xi'=1}^{N_{\mathrm{e}}}\delta_{\boldsymbol{r}^{(\xi)}_\tau,\boldsymbol{r}^{(\xi')}_{\tau'}}\right\} \times \exp\left\{-\Delta\tau\sum_{\tau=1}^{L}\left[U\delta_{\boldsymbol{r}^{(1)}_\tau,\boldsymbol{r}^{(2)}_\tau} + K\sum_{\xi=1}^{N_{\mathrm{e}}}|\boldsymbol{r}^{(\xi)}_\tau|^2\right]\right\}\prod_{\tau=1}^{L}\prod_{\xi=1}^{N_{\mathrm{e}}} I(\boldsymbol{r}^{(\xi)}_{\tau+1} - \boldsymbol{r}^{(\xi)}_\tau). \tag{4}$$

Here $N_{\mathrm{e}} = 1$ (2) for the polaron (bipolaron) problem, and the components of the position vector of electron ξ on time slice τ, $\boldsymbol{r}^{(\xi)}_\tau$, are denoted as $r^{(\xi)}_{\tau,\mu}$ ($\mu = 1, \ldots, \mathrm{D}$). The fermion world-lines are subject to periodic boundary conditions both in real space and imaginary time, and the sum in equation (3) is over all allowed configurations.

The retarded electron (self-)interaction due to electron–phonon coupling is described by the memory function

$$F(\tau) = \frac{\omega_0\Delta\tau^3\alpha^2}{4L}\sum_{\nu=0}^{L-1}\frac{\cos(2\pi\tau\nu/L)}{1-\cos(2\pi\nu/L)+(\omega_0\Delta\tau)^2/2}, \tag{5}$$

and electron hopping contributes

$$I(\boldsymbol{r}) = \frac{1}{N}\sum_{k=0}^{N-1}\cos(\boldsymbol{k}\cdot\boldsymbol{r})\mathrm{e}^{2\Delta\tau t\sum_\mu\cos k_\mu}. \tag{6}$$

3.2. Observables

We define the expectation value of a static observable O as

$$\langle O\rangle = Z^{-1}\mathrm{Tr}\,\hat{O}\mathrm{e}^{-\beta H} = Z_L^{-1}\sum_{\{\boldsymbol{r}^{(\xi)}_\tau\}} O(\{\boldsymbol{r}^{(\xi)}_\tau\})w^{\mathrm{f}}(\{\boldsymbol{r}^{(\xi)}_\tau\}). \tag{7}$$

The fermion contribution to the total energy is obtained from

$$E^{\mathrm{f}} = -\frac{\partial}{\partial\beta}\ln Z^{\mathrm{f}}_L = E^{\mathrm{f}}_{\mathrm{kin}} + E^{\mathrm{f}}_{\mathrm{ep}} + E^{\mathrm{f}}_{\mathrm{ee}} + E^{\mathrm{f}}_{\mathrm{con}} \tag{8}$$

with the kinetic energy ($\boldsymbol{\delta}$ runs over all nearest-neighbour sites)

$$E_{\mathrm{kin}}^{\mathrm{f}} = -\frac{t}{L}\sum_{\tau=1}^{L}\sum_{\xi=1}^{N_{\mathrm{e}}}\sum_{\boldsymbol{\delta}=\mathrm{n.n.}}\left\langle \frac{I(\boldsymbol{r}_{\tau+1}^{(\xi)} - \boldsymbol{r}_{\tau}^{(\xi)} + \boldsymbol{\delta})}{I(\boldsymbol{r}_{\tau+1}^{(\xi)} - \boldsymbol{r}_{\tau}^{(\xi)})}\right\rangle \tag{9}$$

and the interaction energies

$$E_{\mathrm{ep}}^{\mathrm{f}} = -\frac{1}{L}\sum_{\tau,\tau'=1}^{L}\frac{\partial F(\tau-\tau')}{\partial \Delta\tau}\sum_{\xi,\xi'=1}^{N_{\mathrm{e}}}\langle \delta_{\boldsymbol{r}_{\tau}^{(\xi)},\boldsymbol{r}_{\tau'}^{(\xi')}}\rangle, \tag{10}$$

$$E_{\mathrm{ee}}^{\mathrm{f}} = \frac{1}{L}U\sum_{\tau=1}^{L}\langle \delta_{\boldsymbol{r}_{\tau}^{(1)},\boldsymbol{r}_{\tau}^{(2)}}\rangle, \tag{11}$$

and

$$E_{\mathrm{con}}^{\mathrm{f}} = \frac{1}{L}K\sum_{\tau=1}^{L}\sum_{\xi=1}^{N_{\mathrm{e}}}\left\langle |\boldsymbol{r}_{\tau}^{(\xi)}|^2\right\rangle. \tag{12}$$

Also of interest is the electron–lattice correlation function measured in the direction $\mu = 1$,

$$C_{\mathrm{ep}}(r) = (E_{\mathrm{P}}\beta N_{\mathrm{e}})^{-1}\sum_{i=1}^{N}\langle \hat{n}_i\hat{x}_{i+r}\rangle, \qquad r = 0, 1, \ldots, N-1, \tag{13}$$

which fulfils the sum rule $\sum_r C_{\mathrm{ep}}(r) = 1$ (for $E_{\mathrm{P}} > 0$). Within QMC, we have [34]

$$C_{\mathrm{ep}}(r) = (E_{\mathrm{P}}\beta N_{\mathrm{e}})^{-1}\sum_{\tau,\tau'=1}^{L}F(\tau-\tau')\sum_{\xi=1}^{N_{\mathrm{e}}}\langle \delta_{r_{\tau,1}^{(\xi)},r_{\tau',1}^{(\xi)}}\rangle. \tag{14}$$

Similarly, for $N_{\mathrm{e}} = 2$, we calculate the electron–electron correlation function

$$C_{\mathrm{ee}}(r) = \sum_{i=1}^{N}\langle \hat{n}_{i\uparrow}\hat{n}_{i+r\downarrow}\rangle, \qquad r = 0, 1, \ldots, N-1, \tag{15}$$

fulfilling $\sum_r C_{\mathrm{ee}}(r) = 1$, for which the QMC estimator reads

$$C_{\mathrm{ee}}(r) = \frac{1}{L}\sum_{\tau=1}^{L}\langle \delta_{|r_{\tau,1}^{(1)} - r_{\tau,1}^{(2)}|,r}\rangle. \tag{16}$$

3.3. Simulation details

The system described by the partition function (3) is characterized by an additional dimension (imaginary time), as well as by a complicated retarded interaction. As first shown in [32], it may be simulated by means of Markov Chain Monte Carlo in combination with the Metropolis–Hastings algorithm [41]. To improve convergence for critical parameters, we use both local updates (change of a random component of the position vector on a random time slice of one particle by one lattice site) and global updates (translation of an entire world-line by one lattice site) [35].

An important point overlooked in previous work [32–34, 36] is the problem of significant statistical correlations between successive configurations due to the local updating. Whereas previous authors performed measurements every L steps, we find that this is by far not sufficient to ensure statistically independent measurements, especially at intermediate electron–phonon coupling. The integrated autocorrelation time in such cases may well exceed tens of thousands of MC steps, so that a careful binning analysis [42] is required for every run to ensure

correct results and error bars. Details of this problem will be reported elsewhere. Although autocorrelation times are expected to be generally shorter in continuous-time simulations (see, e.g., [43]), the problem must not be neglected. A QMC algorithm entirely free of autocorrelations has been presented in [40, 44], but this approach suffers from restrictions in system size for $D > 1$ [45]. Another problem of world-line algorithms is that the acceptance rate for local updates approaches zero in the strong-coupling regime. For $K/t \gtrsim 1$ and $\lambda \gtrsim 1$, this becomes also true for global updates. Finally, we also detected convergence problems in the vicinity of the small-(bi-)polaron crossover due to critical slowing down.

The only systematic error in the present calculations comes from the Suzuki–Trotter approximation (equation (2)). It may be eliminated by working in continuous imaginary time [43], or by performing simulations at different $\Delta\tau$ and exploiting the $\Delta\tau^2$-dependence of the results to scale to $\Delta\tau = 0$. To save some computer time, here we have simply chosen a single (small) value of $\Delta\tau = 0.05$, which ensures that the Suzuki–Trotter error is satisfactorily small.

4. Results

We discuss our numerical results in relation to the available knowledge of the Holstein–Hubbard model (equation (1) with $K = 0$). Similar to the non-confined case, the adiabaticity ratio γ turns out to have an important effect on the physics, and a comparison of the cases $\gamma \ll 1$ and $\gamma \gg 1$ will be given for the one-dimensional (1D) polaron. In higher dimensions, we shall focus on the adiabatic regime $\gamma \ll 1$, as the low-lying optical phonon energies in quantum dot materials are in the range of 10–100 meV, i.e., substantially smaller than the electron bandwidth.

The 2D (3D) geometry considered here—corresponding to a circular (spherical) quantum dot—may actually be realized experimentally, whereas the 1D case is mainly of theoretical interest. However, we shall see that the physics is qualitatively similar in $D = 1$ and $D > 1$.

All simulations have been carried out using a linear lattice size of $N = 31$, enough to obtain very well converged results even for $K = 0$ [33, 36]. Since for $K > 0$ the local physics becomes more important, finite-size effects are negligible. The centre of the parabolic potential is located at site $i = 0$ of each dimension, and the site indices range over $[-15, 15]$. To study the ground-state properties, we set the inverse temperature $\beta t = 15$. The number of Trotter time slices has been fixed to $L = 300$ so that $\Delta\tau = 0.05$. Errorbars are typically smaller than the linewidth, and are shown only if they are larger than the symbols used.

A drawback of the present approach (cf [43, 46]) is that we cannot calculate the quasiparticle effective mass. Instead, we shall consider the electronic kinetic energy, which includes contributions from incoherent processes. Additionally, the correlation functions defined in section 3 permit us to monitor the size of the (bi-)polaron, and to determine the critical coupling for the crossover to a small-(bi-)polaron state.

The confinement length—often a directly tunable parameter in previous work—is set by the oscillator strength ($\sim K$) of the harmonic potential. For two electrons, it may be estimated from the electron–electron correlation function $C_{\mathrm{ee}}(r)$ at $\lambda = 0$.

4.1. Polaron

Existing work suggests that the ground state of the Holstein model with one electron ($K = 0$, U irrelevant) at weak electron–phonon coupling is a large polaron (extending over more than one lattice site) in one dimension, and a quasi-free electron for $D > 1$ [47].

With increasing coupling λ, the potential energy due to lattice deformation increases relative to the kinetic energy of the electron. In the adiabatic regime $\gamma < 1$, a small-polaron

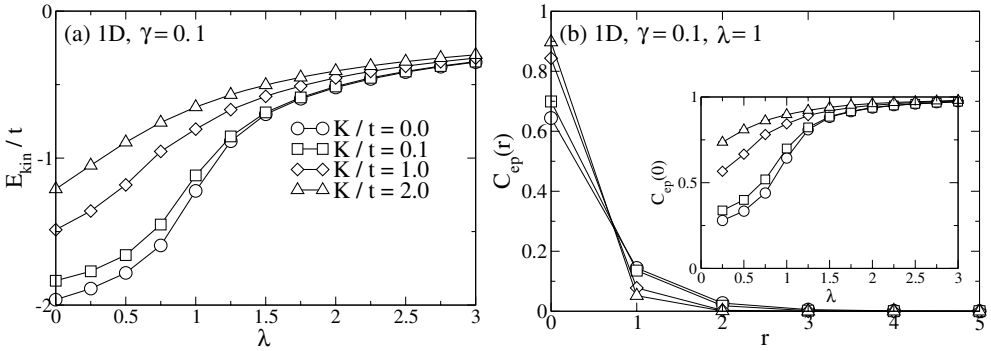

Figure 1. (a) Kinetic energy $E_{\rm kin}$ of one electron in a 1D system in the adiabatic regime ($\gamma = 0.1$) as a function of electron–phonon coupling strength λ for different values of the confinement strength K. Here and in subsequent figures $N = 31$, $\beta t = 15$ and $\Delta\tau = 0.05$. Lines are guides to the eye only. (b) Electron–lattice correlation function $C_{\rm ep}(r)$ as a function of distance r for the same parameters as in (a) and $\lambda = 1$. The inset shows $C_{\rm ep}(0)$ as a function of λ.

state (with the electron and the lattice distortion being localized essentially to the same site) is formed if $E_{\rm P} > W/2$ ($\lambda > 1$). In contrast, for $\gamma > 1$, small-polaron formation requires a sizeable lattice distortion, leading to the condition $g^2 = E_{\rm P}/\omega_0 > 1$. Note that these 'critical couplings' are conceptually different from those for the occurrence of the Peierls quantum phase transition at half-filling [52] since there is no phase transition in the (bi-)polaron problem for $\gamma > 0$ [48].

The small-polaron state is characterized by a substantially enhanced effective mass and corresponding small quasiparticle weight. Generally, the size of the polaron is smaller in the non-adiabatic strong-coupling regime due to the faster lattice response.

4.1.1. One dimension. Figure 1(a) shows results for a single electron in a 1D system for $\gamma = 0.1$. For $K = 0$, starting with the non-interacting value $-2t$, the absolute value of the kinetic energy is reduced with increasing λ. The crossover near $\lambda = 1$ is continuous (the same also applies in higher dimensions [48]).

Turning on the confinement, we see that results are very similar for small $K/t = 0.1$ (weak confinement). Remarkably, in the case of strong confinement—the size of the quantum dot is very small for $K/t = 2$—the kinetic energy displays the convex behaviour characteristic of the strong-coupling regime already near $\lambda = 0$. This may be understood as a result of squeezing of the polaron state: for weak coupling, the free ($K = 0$) polaron size is larger than the dot size set by K, so the kinetic energy is determined mainly by the confinement. In contrast, for strong coupling, the polaron size is smaller than the dot size and the kinetic energy is almost identical to the case $K/t = 0$. Therefore, all curves tend to the same value $-2tI(1)/I(0)$ as $\lambda \to \infty$.

The effect of the confinement on the polaron size at the critical coupling $\lambda = 1$ (for $K = 0$) is illustrated by the results for the electron–lattice correlation function $C_{\rm ep}(r)$ in figure 1(b). For small K, the lattice distortion surrounding the electron extends over about two lattice sites (large polaron). The effect of confinement is to reduce the polaron size, as is well visible especially for $K/t = 2$.

In the inset of figure 1(b) we present data for $C_{\rm ep}(0)$ as a function of λ. As pointed out in [49], the small-polaron crossover occurs at the point where the slope of $C_{\rm ep}(0)$ has its maximum, which in the present case confirms the critical coupling $\lambda = 1$ obtained from energetic considerations ($K = 0$). Furthermore, numerical differentiation of the data shown

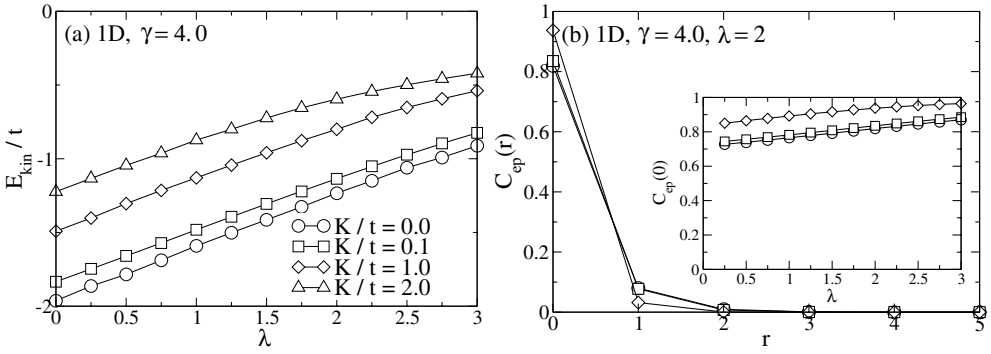

Figure 2. As in figure 1 but for the anti-adiabatic regime ($\gamma = 4$).

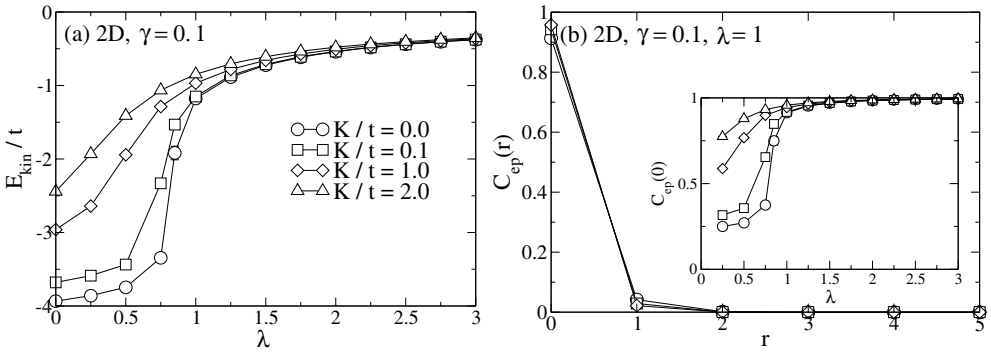

Figure 3. As in figure 1 but for a 2D system.

clearly indicates that the critical coupling is reduced by about 50% in the strong confinement regime $K/t \geqslant 1$ owing to the smaller non-interacting ($\lambda = 0$) kinetic energy.

Figure 2 shows results for the anti-adiabatic regime ($\gamma = 4$). For $K = 0$, the kinetic energy in (a) shows a very smooth dependence on the electron–phonon coupling strength. The critical value for the small-polaron crossover is given by $g^2 = 1$ ($\lambda = 2$), but no pronounced changes in $E_{\rm kin}$ are visible. For $K > 0$, the form of the kinetic energy curve does not change noticeably, because the free polaron size is smaller than the confinement length even for $g^2 < 1$.

The electron–lattice correlation function in figure 2(b) confirms the smaller size of the polaron at the $K = 0$ critical coupling (cf figure 1(b)). Consequently, the dependence on K is much weaker than in the adiabatic regime. As for $\gamma = 0.1$, the critical coupling for small-polaron formation is substantially reduced for large K/t, as can be inferred from the slope of $C_{\rm ep}(0)$.

4.1.2. Higher dimensions. For the non-confined case, it is known that the small-polaron crossover becomes more abrupt as a function of λ in higher dimensions. This is well visible from the 2D results for $E_{\rm kin}$ shown in figure 3(a), as well as from the inset of figure 3(b).

The effect of confinement is again a reduction of the kinetic energy. For $K/t = 2$, the convex strong-coupling behaviour is seen to be similar to $D = 1$. An important difference to the 1D case is that the curves for different K become practically indistinguishable for $\lambda > 2$,

Table 1. Conditions for the existence of different singlet bipolaron states in the one-dimensional Holstein–Hubbard model at weak (WC) and strong electron–phonon coupling (SC) [38, 40].

$U = 0$		$U > 0$		
Large bipolaron	Small bipolaron	Two polarons	Inter-site bipolaron	Small bipolaron
$\lambda < 0.5$ ($\gamma < 1$) or $g < 0.5$ ($\gamma > 1$)	$\lambda > 0.5$ ($\gamma < 1$) and $g > 0.5$ ($\gamma > 1$)	$U > 2E_\mathrm{P}$ (WC) $U > 4E_\mathrm{P}$ (SC)	$U < 2E_\mathrm{P}$ (WC) $U < 4E_\mathrm{P}$ (SC)	$U \ll 2E_\mathrm{P}$

whereas in one dimension (figure 1(a)) such a collapse occurs for $\lambda \gtrsim 3$. The origin of this effect is revealed in figure 3(b). Obviously, the polaron is smaller in two dimensions than in one dimension for the same λ, reducing the effect of K. The inset again reveals a reduction of the critical coupling with increasing confinement. Similar behaviour is also found in three dimensions (not shown), with an even stronger dependence of E_kin and $C_\mathrm{ep}(r)$ on λ.

Let us discuss the relation of our results to previous work. The common conclusion is that the confinement demobilizes the carrier, which manifests itself either in an increase of effective mass, or a decrease of kinetic energy and the polaron size [20–24]. Also in accordance with existing work, we find that the polaronic correction to the total energy is larger for larger K. For example, $\Delta E^\mathrm{f} = [E^\mathrm{f}_{\lambda=0} - E^\mathrm{f}_{\lambda=1}]/E^\mathrm{f}_{\lambda=0} \approx 0.54$ for $K/t = 0.1$, whereas $\Delta E^\mathrm{f} \approx 1.08$ for $K/t = 2$.

The reduction of the critical coupling for the existence of a small polaron due to confinement complies with the growth of the strong-coupling region at the expense of the weak-coupling region in the phase diagram pointed out in [23].

Furthermore, we observe a similar dependence of the influence of confinement on dimensionality as for the continuum model [22] (in this work the effective mass was considered). Comparing the values of the kinetic energy at $\lambda = 1$, we find for the ratio $E_\mathrm{kin}(K)/E_\mathrm{kin}(K = 0) = 0.91$ ($K/t = 0.1$), 0.66 ($K/t = 1$), and 0.53 ($K/t = 2$) in one dimension, and 0.98, 0.82, and 0.72 in two dimensions. Hence, confinement effects are significantly stronger in one dimension than in two dimensions, and this trend extends to $D = 3$.

4.2. Bipolaron

We now come to the case of two electrons of opposite spin, which can form a bound bipolaron state given sufficiently strong electron–phonon interaction. Owing to the Coulomb repulsion, the physics becomes much richer, and we again begin our discussion with the 1D case.

Compared to the one-electron problem, significantly less work has been done on the bipolaron problem in the framework of the Holstein–Hubbard model. Nevertheless, from existing studies (see [30, 39, 40, 50] and references therein), the basic physics is understood. A summary of (approximate) conditions for the existence of the different ground states is given in table 1.

4.2.1. One dimension. Figure 4 shows results for the simplest case $U = 0$, in the adiabatic regime ($\gamma = 0.1$). For $K = 0$, the two electrons form a bound state if $4E_\mathrm{P} > 4t$ ($\lambda > 0.5$), where $4E_\mathrm{P}$ is the bipolaron binding energy in the atomic limit and $4t$ is the free kinetic energy of the two electrons. The corresponding crossover from a large bipolaron (no unbound polarons exist for $U = 0$) to a small (on-site) bipolaron leads to a noticeable decrease of the (absolute)

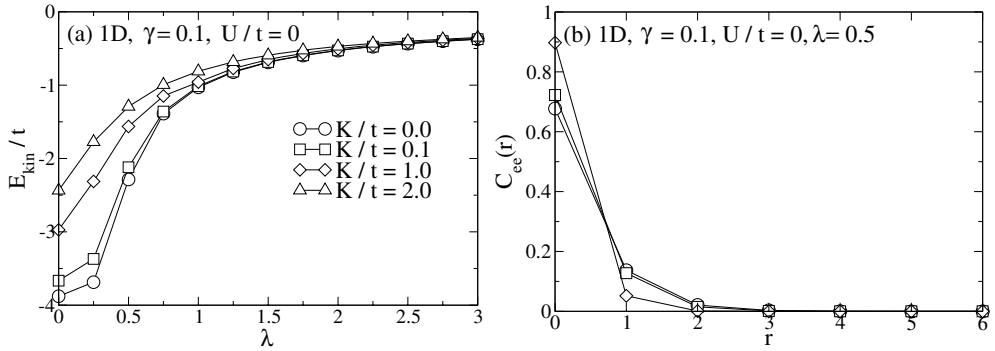

Figure 4. (a) Kinetic energy $E_{\rm kin}$ of two electrons in a 1D system in the adiabatic regime ($\gamma = 0.1$) for $U = 0$ as a function of electron–phonon coupling strength λ for different values of the confinement strength K. (b) Electron–electron correlation function $C_{\rm ee}(r)$ as a function of distance r for the same parameters as in (a) and $\lambda = 0.5$.

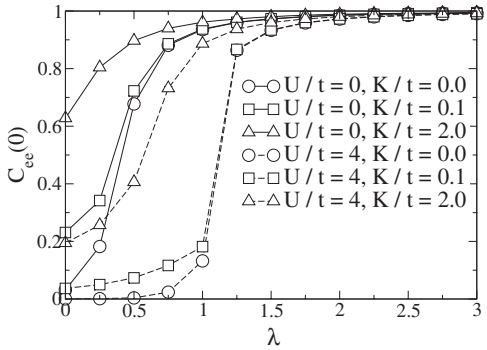

Figure 5. Electron–electron correlation function $C_{\rm ee}(0)$ as a function of electron–phonon coupling strength λ for a 1D system, $\gamma = 0.1$, and different values of the Hubbard repulsion U and the confinement strength K.

kinetic energy in figure 4(a). As for the polaron, the critical value for the crossover may be determined from the slope of $C_{\rm ep}(0)$ or $C_{\rm ee}(0)$ (see figure 5).

Apart from enforcing polaron effects, confinement enhances the probability for the two electrons to occupy the same region of the system (the vicinity of the centre of the harmonic potential). This in turn leads to a stronger pairing tendency. Any $K/t > 0$ decreases the kinetic energy in the weak- and intermediate-coupling regimes. For strong confinement, the kinetic energy exhibits the typical strong-coupling dependence on λ. The reduction of the bipolaron size (the average distance between the two carriers) due to confinement is shown in figure 4(b) for the free critical coupling $\lambda = 0.5$. Finally, figure 5 reveals that the critical coupling for small-bipolaron formation is substantially smaller in a strongly confined system.

It is more realistic to consider the case of finite Coulomb repulsion $U/t = 4$. For $K = 0$, strong-coupling theory predicts a ground state with two unbound (large) polarons for $2E_{\rm P} \lesssim U$. In the vicinity of $2E_{\rm P} = U$, the so-called inter-site bipolaron exists, with the electrons being most likely to occupy neighbouring lattice sites, and with only slightly enhanced effective mass as compared to two unbound polarons [37, 38, 40]. The origin of this state is a non-local

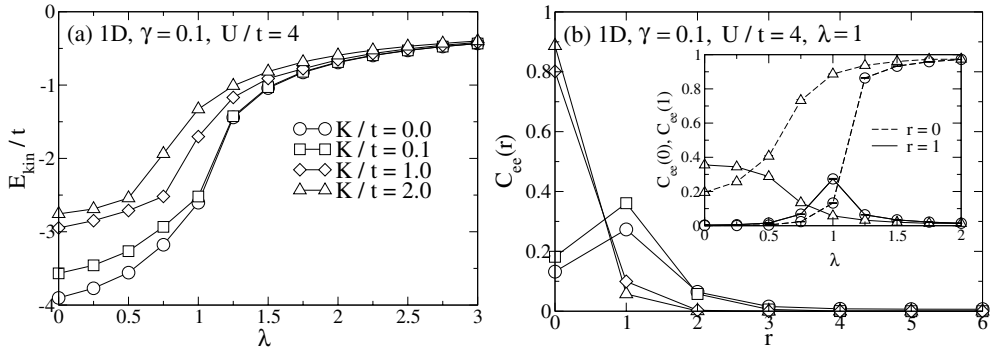

Figure 6. As in figure 4 but for $U/t = 4$. The inset in (b) shows the electron–electron correlation functions $C_{\rm ee}(0)$, $C_{\rm ee}(1)$.

exchange interaction process [38] which allows the particles to gain potential energy from the coupling to phonons, and at the same time avoid the penalty due to Hubbard repulsion.

Remarkably, figure 6(a) reveals a critical coupling for the small-bipolaron crossover of $2E_{\rm P} \approx U$ ($\lambda \approx 1$, see also the inset of figure 6(b)), which is in a surprisingly good agreement with the anti-adiabatic strong-coupling condition (despite $\gamma = 0.1$). Our findings extend previous calculations limited either to $\gamma = 1$ [38] or small systems [40], and a phase diagram for the important adiabatic regime will be presented elsewhere.

As for $U = 0$, confinement leads to a reduction of the kinetic energy and the average distance between the two electrons (figure 6(b)). However, owing to the on-site repulsion, the results for $E_{\rm kin}$ exhibit weak and strong-coupling behaviour even for $K/t = 2$.

An interesting point concerns the effect of confinement on the inter-site state. The inset in figure 6(b) shows the electron–electron correlation functions $C_{\rm ee}(0)$ and $C_{\rm ee}(1)$. For $K = 0$, in the vicinity of $\lambda = 1$, $C_{\rm ee}(1) > C_{\rm ee}(0)$ as characteristic for the inter-site bipolaron. In contrast, for strong confinement $K/t = 2$, the region of existence of the latter is limited to small λ. Clearly, for sufficiently strong confinement, the inter-site state will disappear.

In previous strong-coupling calculations in the framework of the continuum model [24–26], it has been found that the bound bipolaron state becomes unstable at very strong confinement, which was attributed to the increase of the Coulomb interaction energy for two spatially close particles. However, this effect has been argued [23, 26] to be due to the approximations made, and path-integral calculations [23] as well as analytical and QMC calculations [17] suggest that a bound state also exists at weak coupling in a confined system.

Preliminary calculations of the bipolaron binding energy $E^{\rm f}(N_{\rm e} = 2) - 2E^{\rm f}(N_{\rm e} = 1)$ for $\gamma = 0.1$ and $U/t = 4$ at $K/t = 0.1$ and $K/t = 2.0$ in one dimension reveal that a weakly bound bipolaron can indeed become unbound due to confinement. This effect of on-site Coulomb interaction is expected to be most pronounced in one dimension, and this issue will be further investigated in future work.

It is worth mentioning the relation of our calculations to recent work on molecular quantum dots [18, 19] based on models with a single molecular level and a vibrational mode, weakly coupled to metallic leads. In such systems, the bipolaron binding energy can compensate for the Hubbard repulsion U, giving rise to a net attraction and thereby favouring pair tunnelling of electrons. Due to the absence of a sizable hopping amplitude, the ground-state properties of such a single-site molecule are determined mainly by the atomic-limit physics of the present model. In particular, the inter-site bipolaron state will be strongly suppressed, and the strong-

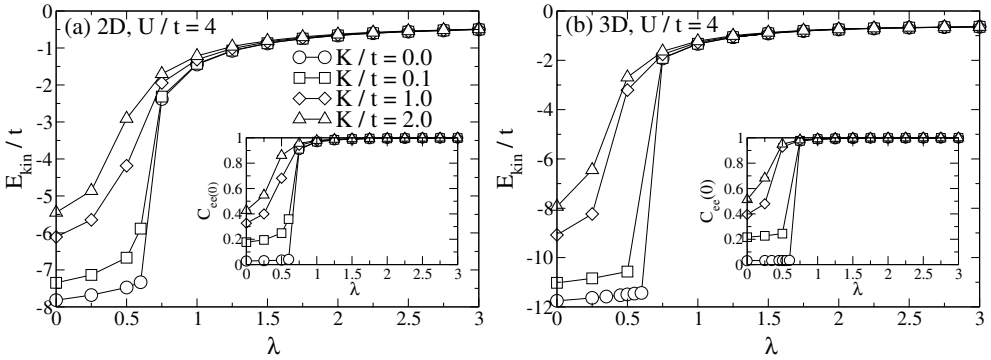

Figure 7. Kinetic energy $E_{\rm kin}$ for two electrons in the adiabatic regime ($\gamma = 0.1$) for $U/t = 4$ as a function of coupling strength λ for different values of the confinement strength K in (a) two dimensions, (b) three dimensions. The insets show the electron–electron correlation function $C_{\rm ee}(r = 0)$ versus λ.

coupling criteria of table 1 are expected to hold. The situation may be expected to be different for finite-size molecules.

4.2.2. Higher dimensions. Numerical results for the unconfined Holstein–Hubbard model in $D > 1$ have been reported before in two dimensions for $\gamma = 1$ [39], and in three dimensions for classical phonons [35], but no reliable results are available for the important adiabatic regime $\gamma \ll 1$. We restrict the discussion to the more general case $U > 0$.

As in the polaron problem, the crossover to a small bipolaron becomes more pronounced in higher dimensions (note the different ordinate scales in figures 6(a), 7(a) and (b)). The critical coupling for $K = 0$ from the strong-coupling approximation is again set by $U \approx 2E_{\rm P}$, corresponding to $U/W = \lambda$. Indeed, for $D = 2$ (figure 7(a)), we find the crossover near $\lambda = 0.5$, in agreement with this condition. However, in three dimensions, the crossover occurs slightly above $\lambda = 0.5$, whereas the strong-coupling result yields $\lambda = 0.33$. This deviation may be explained by the larger number of nearest-neighbour sites in three dimensions, which may enhance the stability of extended (inter-site) bipolaron states.

Confinement again leads to a reduction of the critical coupling, as well as to an enhancement of bipolaron effects. As for a single electron, we can calculate the change of the kinetic energy with confinement (relative to $K = 0$) at $\lambda = 1$. This yields 0.89 in two dimensions, and 0.95 in three dimensions, so we can conclude that confinement effects are again more noticeable in lower dimensions.

5. Summary and outlook

Unbiased quantum Monte Carlo studies of the Holstein–Hubbard model with additional harmonic confinement on a discrete lattice have been carried out in one to three dimensions, considering the cases of one and two electrons. Technical difficulties encountered in simulations using the present world-line method, some of which were overlooked in previous work, have been revealed.

The effect of confinement on the formation of polarons and bipolarons has been investigated. Despite considerable simplifications inherent to the model, we believe that our exact numerical results are relevant for quantum dot systems.

In addition to providing unbiased results for all physically relevant parameter regimes, we have for the first time reported on results for a (multi-site) cluster model of a quantum dot. The latter is particularly important for the very small dots which can be fabricated today, as well as for a description of the small-(bi-)polaron crossover associated to a local lattice instability. Quantum phonon effects and electron–electron interaction were fully taken into account.

For one electron, we find that the basic effect of confinement consists in enhancing polaronic effects—the polaron size and the critical coupling for the existence of a small polaron both decrease. The influence of confinement is largest in a 1D system in the adiabatic regime, and becomes significantly smaller with increasing dimension or phonon frequency. In the strongly confined regime, the polaron state is squeezed, giving rise to small-polaron physics even for weak or intermediate coupling.

We have presented the first accurate results for the unconfined Holstein–Hubbard bipolaron in the adiabatic regime in more than one dimension. We find indications that confinement can counteract bipolaron formation in the presence of Coulomb repulsion, but this issue needs further investigation also in the framework of a model with long-range interactions. For finite on-site repulsion, weak-coupling behaviour survives even for strong confinement.

Existing work on (bi-)polarons in quantum dots is almost exclusively restricted to equilibrium properties, although most technical applications fall into the non-equilibrium regime. Since the fundamental effects of confinement on the ground state are now rather well understood, it is desirable to consider more general situations in the future. Apart from effects due to long-range interactions and anharmonic confinement in cluster models, this includes many-polaron effects [51], and coupling of electrons or excitons to light [16], as well as transport properties and time-dependent phenomena. Of course, suitable numerical methods will have to be developed to address these problems, and work along these lines is in progress.

Acknowledgments

We gratefully acknowledge financial support by the Austrian Science Fund (FWF) through the Erwin-Schrödinger Grant No J2583, the Deutsche Forschungsgemeinschaft through SFB 652, KONWIHR, and the European Science Foundation. We thank H de Raedt for valuable correspondence, and G Hager and G Wellein for useful discussion. Furthermore, we acknowledge generous computing time at the TU Graz and the Computing Centre Erlangen.

References

[1] Jacak L, Hawrylak P and Wójs A 1998 *Quantum Dots* (New York: Springer)
[2] Yoffe A D 2001 *Adv. Phys.* **50** 1
[3] Kouwenhoven L and Marcus C 1998 *Phys. World* **11** 35
[4] Akiyama H 1998 *J. Phys.: Condens. Matter* **10** 3095
[5] Li X, Wu Y, Steel D, Gammon D, Stievater T H, Katzer D S, Park D, Piermarocchi C and Sham L J 2003 *Science* **301** 809
[6] Kroutvar M, Ducommun Y, Heiss D, Bichler M, Schuh D, Abstreiter G and Finley J J 2004 *Nature* **432** 81
[7] Michler P, Kiraz A, Becher C, Schoenfeld W V, Petroff P M, Zhang L, Hu E and Imamoğlu A 2000 *Science* **290** 2282
[8] Pelton M, Santori C, Vuckovic J, Zhang B and Solomon G S 2002 *Phys. Rev. Lett.* **89** 233602
[9] Flissikowski T, Hundt A, Lowisch M, Rabe M and Henneberger F 2001 *Phys. Rev. Lett.* **86** 3172
[10] Liang W, Shores M P, Bockrath M, Lond J R and Park H 2002 *Nature* **417** 725
[11] Inoshita T and Sakaki H 1992 *Phys. Rev.* B **46** 7260
[12] Pazy E 2002 *Semicond. Sci. Technol.* **17** 1172
[13] Muljarov E A and Zimmermann R 2004 *Phys. Rev. Lett.* **93** 237401
[14] Wu B H and Cao J C 2004 *J. Phys.: Condens. Matter* **16** 8285

[15] Hameau S, Guldner Y, Verzelen O, Ferreira R and Bastard G 1999 *Phys. Rev. Lett.* **83** 4152
[16] Preisler V, Grange T, Ferreira R, de Vaulchier L A, Guldner Y, Teran F J, Potemski M and Lemaître A 2006 *Phys. Rev.* B **73** 075320
[17] Wan Y, Ortiz G and Phillips P 1997 *Phys. Rev.* B **55** 5313
[18] Alexandrov A S and Bratkovsky A M 2003 *Phys. Rev.* B **67** 235312
[19] Koch J, Raikh M E and von Oppen F 2006 *Phys. Rev. Lett.* **96** 056803
[20] Yildirim T and Erçelebi A 1991 *J. Phys.: Condens. Matter* **3** 1271
[21] Yildirim T and Erçelebi A 1991 *J. Phys.: Condens. Matter* **3** 4357
[22] Sahoo S 1996 *Z. Phys.* B **101** 97
[23] Pokatilov E P, Fomin V M, Devreese J T, Balaban S N and Klimin S N 1999 *J. Phys.: Condens. Matter* **11** 9033
[24] Chatterjee A and Mukhopadhyay S 2001 *Acta Phys. Pol.* B **32** 473
[25] Mukhopadhyay S and Chatterjee A 1996 *J. Phys.: Condens. Matter* **8** 4017
[26] Senger R T and Erçelebi A 2000 *Eur. Phys. J.* B **16** 439
[27] Fröhlich H 1954 *Adv. Phys.* **3** 325
[28] Holstein T 1959 *Ann. Phys.* **8** 325
Holstein T 1959 *Ann. Phys.* **8** 343
[29] Ranninger J 2006 Polarons in bulk materials and systems with reduced dimensionality *Proc. Int. School of Physics Enrico Fermi, Course CLXI (Oxford, Tokio, Washington DC)* ed G Iadonisi, J Ranninger and G De Filippis (Amsterdam: IOS Press) pp 1–25
[30] Alexandrov A S and Mott N 1995 *Polarons & Bipolarons* (Singapore: World Scientific)
[31] Fehske H, Alvermann A, Hohenadler M and Wellein G 2006 Polarons in bulk materials and systems with reduced dimensionality *Proc. Int. School of Physics Enrico Fermi, Course CLXI (Oxford, Tokyo, Washington, DC)* ed G Iadonisi, J Ranninger and G De Filippis (Amsterdam: IOS Press) pp 285–96
[32] De Raedt H and Lagendijk A 1982 *Phys. Rev. Lett.* **49** 1522
[33] De Raedt H and Lagendijk A 1983 *Phys. Rev.* B **27** 6097
[34] De Raedt H and Lagendijk A 1984 *Phys. Rev.* B **30** 1671
[35] De Raedt H and Lagendijk A 1986 *Z. Phys.* B **65** 43
[36] Kornilovitch P E 1997 *J. Phys.: Condens. Matter* **9** 10675
[37] Weiße A, Fehske H, Wellein G and Bishop A R 2000 *Phys. Rev.* B **62** R747
[38] Bonča J, Katrašnik T and Trugman S A 2000 *Phys. Rev. Lett.* **84** 3153
[39] Macridin A, Sawatzky G A and Jarrell M 2004 *Phys. Rev.* B **69** 245111
[40] Hohenadler M and von der Linden W 2005 *Phys. Rev.* B **71** 184309
[41] Metropolis N, Rosenbluth A, Teller A and Teller E 1953 *J. Chem. Phys.* **21** 1087
[42] Evertz H G 2003 *Adv. Phys.* **52** 1
[43] Kornilovitch P E 1998 *Phys. Rev. Lett.* **81** 5382
[44] Hohenadler M, Evertz H G and von der Linden W 2004 *Phys. Rev.* B **69** 024301
[45] Hohenadler M, Evertz H G and von der Linden W 2005 *Phys. Status Solidi* b **242** 1406
[46] Prokof'ev N V and Svistunov B V 1998 *Phys. Rev. Lett.* **81** 2514
[47] Kabanov V V and Mashtakov O Yu 1993 *Phys. Rev.* B **47** 6060
[48] Löwen H 1988 *Phys. Rev.* B **37** 8661
[49] Capone M, Ciuchi S and Grimaldi C 1998 *Europhys. Lett.* **42** 523
[50] Hohenadler M, Aichhorn M and von der Linden W 2005 *Phys. Rev.* B **71** 014302
[51] Hohenadler M, Hager G, Wellein G and Fehske H 2007 *J. Phys.: Condens. Matter* **19** 255202
[52] Hohenadler M, Wellein G, Bishop A R, Alvermann A and Fehske H 2006 *Phys. Rev.* B **73** 245120